Energy Optimal Waypoint Guidance Synthesis for Antiship Missiles

CHANG-KYUNG RYOO
Inha University

HYO-SANG SHIN

MIN-JEA TAHK
Korea Advanced Institute of Science and Technology

Planar waypoint guidance synthesis methods for antiship missiles (ASMs) using optimal guidance laws are proposed. The energy optimal trajectory optimization problem with waypoint constraints is converted to an unconstrained optimization problem of finding the optimal boundary conditions at waypoints for the guidance laws. An optimal guidance law (OGL) for a 1st-order lag ASM with terminal constraints on the impact angle and lateral acceleration is newly proposed for this purpose. The proposed method produces the energy optimal trajectory with high numerical efficiency. If the ASM is approximated by a lag-free system, optimal boundary conditions become waypoint passing angles which can be simply determined from a set of linear algebraic equations. Since there are no time-consuming numerical optimizations in this approach, the energy optimal trajectory passing through all the waypoints can be generated in real time.

Manuscript received October 10, 2005; revised October 1, 2006 and May 8, 2008; released for publication August 24, 2008.

IEEE Log No. T-AES/46/1/935929.

Refereeing of this contribution was handled by Y. Oshman.

This work was supported by Inha University Research Grant INHA-36618.

Authors' addresses: C-K. Ryoo, Dept. of Aerospace Engineering, Inha University, 253 Yonghyun-Dong, Nam-Gu, Incheon, 402-751, Korea; H-S. Shin and M-J. Tahk, Dept. of Aerospace Engineering, Korea Advanced Institute of Science and Technology, 373-1 Guseong Yuseong, Daejeon, 305-701, Korea, E-mail: (mjtahk@fdcl.kaist.ac.kr).

I. INTRODUCTION

Typical antiship missiles (ASMs) perform sea skimming at a prescribed altitude in order to enhance survivability. Path planning and guidance of the ASM on the horizontal plane are also important to avoid obstacles such as islands and antiair threats and to deceive the enemy. Trajectory optimization to minimize control energy [1, 2] or flight time [3, 4] has been adopted to meet such demands. However, this approach is available only for predetermined missions, because real-time trajectory optimization remains a challenging research area. Furthermore, this approach requires a path regulator to put the ASM on the predetermined path.

As shown in Fig. 1, complex ASM missions can be easily accomplished by waypoint guidance. The purpose of waypoint guidance is to deliver the ASM from one waypoint to the next waypoint in a given order. By regarding the next waypoint as a fixed target, typical missile guidance laws can be directly used for waypoint guidance. As an example, proportional navigation guidance (PNG, [5]) can be used for waypoint guidance. For PNG, however, the guidance command is abruptly changed when the next waypoint is newly assigned as a target, and trajectory shaping to satisfy path constraints is not flexible. In [6], line-of-sight (LOS) waypoint guidance is proposed for autonomous marine vehicles. In this method, the LOS connecting the current waypoint and the next waypoint is imbedded in the guidance synthesis method for a smooth command transition.

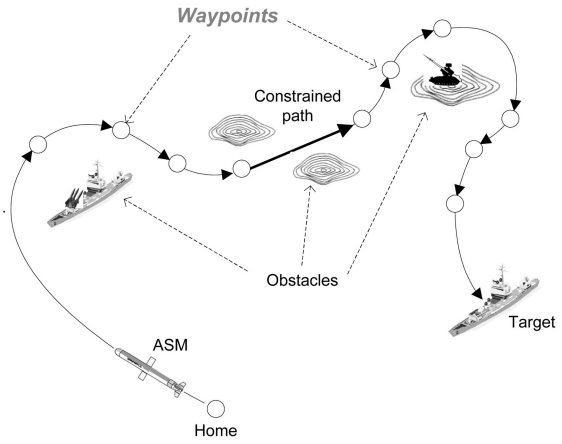

Fig. 1. Path planning example of ASM missions.

In [7], a waypoint guidance algorithm to follow the straight-line segment between two waypoints is proposed. The basic idea of this method is to regulate the flight path along the line segment by a linear quadratic regulator (LQR) and to transfer the vehicle to the next line-segment with the minimum acceleration turn. The application of this method, however, is restricted to line-following missions. The

waypoint guidance method is flexible for in-flight demand of waypoint change. However, this method is completely ad hoc and it is difficult to assign any optimality to this approach. In general, despite that a guidance law has optimality, mere application of the guidance law to each flight region between the waypoints, does not provide optimality of the entire trajectory including all waypoints. In this paper, a waypoint guidance synthesis method based on energy optimal guidance laws (OGLs) is proposed. As the mission range of ASMs gradually expands, minimizing fuel consumption becomes a key factor in waypoint guidance. Energy optimality is also important for ASMs in practical applications. Since guidance command is realized by aerodynamic force, energy-optimized control directly minimizes aerodynamic drag as well as the size of the actuator system. The size of the actuator system depends on the maximum required power which is denoted by the control energy per unit time.

We first show that the optimization problem of an energy optimal trajectory passing through all the waypoints in a given order can be converted to an unconstrained parameter optimization problem of finding the optimal boundary conditions at waypoints, under the assumption that a proper OGL exists. If the ASM can be approximated by a 1st-order lag system, then the boundary conditions are the waypoint passing angles and the lateral accelerations. We newly derive the energy OGL for a 1st-order lag system with constraints on the impact angle and terminal lateral acceleration, called OGL-T&A. OGL-T&A is then used for delivering the 1st-order lag ASM from one waypoint to the next waypoint. The remaining problem is how to obtain the optimal waypoint passing angles and lateral accelerations such that the entire trajectory is energy optimal; that is, the original trajectory optimization problem becomes a parameter optimization problem. This approach provides a very efficient and robust numerical methodology to produce the energy optimal trajectory passing all the waypoints.

If the response of the ASM is so fast that it can be approximated by a lag-free system, OGL-T&A can be simplified as the OGL with an impact angle constraint, called OGL/0 [8]. Then, only the waypoint passing angles are the boundary conditions that should be determined for obtaining the energy optimal trajectory. Using the analytic time solution of OGL/0, we can approximate the energy cost as a quadratic function of the waypoint passing angles. By differentiating the energy cost by the waypoint passing angles, simple linear algebraic equations to calculate the suboptimal waypoint passing angles are derived. The energy optimal waypoint guidance is synthesized in two steps: the suboptimal waypoint passing angles are first calculated by using linear algebraic equations, and OGL/0 is then applied to guide the

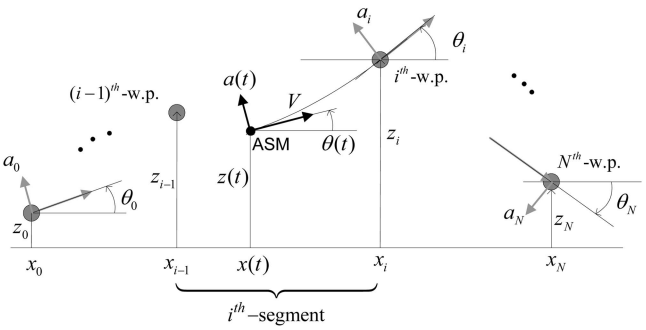

Fig. 2. Geometry of planar waypoint guidance.

ASM between two adjacent waypoints. Since the proposed method does not require any numerical optimization processes, the optimal trajectory can be generated in real time even under sudden changes of the waypoint set, which may be necessary to avoid pop-up threats or to meet mission changes during the flight.

II. EQUIVALENCE OF OPTIMAL CONTROL PROBLEMS

In this paper, we address waypoint guidance and optimal trajectory generation of an ASM. Most long-range ASMs perform sea skimming flight with a constant speed for enhancing survivability in the midcourse phase. Sea skimming altitude and speed are maintained by a height channel autopilot and an engine controller, respectively. Hence, only the problem of the 2-D planar trajectory of the ASM needs to be concerned.

In general, the bandwidth of a guidance loop becomes narrower as the vehicle approaches target and eventually blows up near the bandwidth of the autopilot lag of the vehicle [9]. Therefore, a 1st-order approximation of the vehicle autopilot is enough to identify the characteristics of a guidance law in the conservative point of view. Moreover, a higher order approximation of the autopilot makes it difficult to obtain the analytical solution of an optimal control problem. In these reasons, we assume that $V(t)$, the speed of the ASM, is constant and $a(t)$, the lateral acceleration, is realized by a 1st-order lag system with the time constant τ for the control input $u(t)$.

Consider N waypoints that will be visited by the ASM in a given order as shown in Fig. 2. We define the flight segment between the $(i-1)$th—and the ith-waypoint as the ith-segment. The position of the ith-waypoint, the passing angle, and the lateral acceleration at the ith-waypoint are represented as (x_i, z_i), θ_i, a_i, respectively. $(x(t), z(t))$ and $\theta(t)$ respectively denote the position and the flight path angle of the ASM at t.

Now, consider the following energy optimal control problem.

OCP-1: Find $u(t)$ which minimizes

$$J = \int_0^{t_f} [u(t)]^2 dt = \sum_{i=1}^{N} \int_{t_{i-1}}^{t_i} [u(t)]^2 dt \tag{1}$$

subject to

$$\begin{aligned} \dot{x} &= V\cos\theta \\ \dot{z} &= V\sin\theta \\ \dot{\theta} &= a/V \\ \dot{a} &= (u-a)/\tau \end{aligned} \tag{2}$$

with the constraints of

$$x(t_i) = x_i \qquad \text{and} \qquad z(t_i) = z_i \qquad \text{for} \quad i = 0,1,\ldots,N. \tag{3}$$

where t_i is defined as the time when the ASM reaches the ith-waypoint. By definition, $t_0 = 0$ and $t_N = t_f$.

In OCP-1, different optimal control will be obtained according to t_i if t_i is fixed. Hence, t_i in OCP-1 must not be fixed in order to obtain the optimal control that globally minimizes the cost.

Let the cost of each segment in (1) be defined by

$$J_i \triangleq \int_{t_{i-1}}^{t_i} [u(t)]^2 dt \qquad \text{for} \quad i = 1,2,\ldots,N \tag{4}$$

and $u^*(t)$ be the solution to OCP-1. The minimum cost J^* can then be represented by

$$J^* = \sum_{i=1}^{N} J_i^* \tag{5}$$

where

$$J_i^* \triangleq \int_{t_{i-1}}^{t_i} [u^*(t)]^2 dt \qquad \text{for} \quad i = 1,2,\ldots,N. \tag{6}$$

Consider another optimal control problem with the terminal constraints on the zero miss distance, the desired passing angle, and the terminal lateral acceleration for the ith-segment.

OCP-2: For the given time interval $[t_{i-1}, t_i]$, find $\bar{u}(t)$ that minimizes

$$\bar{J}_i = \int_{t_{i-1}}^{t_i} [\bar{u}(t)]^2 dt \tag{7}$$

subject to (2) with the initial conditions,

$$\begin{aligned} x(t_{i-1}) &= x_{i-1}, \qquad z(t_{i-1}) = z_{i-1} \\ \theta(t_{i-1}) &= \theta_{i-1}, \qquad a(t_{i-1}) = a_{i-1} \end{aligned} \tag{8}$$

and the terminal constraints,

$$\begin{aligned} x(t_i) &= x_i, \qquad z(t_i) = z_i \\ \theta(t_i) &= \theta_i, \qquad a(t_i) = a_i. \end{aligned} \tag{9}$$

Let $\bar{u}^*(t)$ be the solution to OCP-2; the minimum cost $\bar{J}_i^*$ is then obtained as

$$\bar{J}_i^* = \int_{t_{i-1}}^{t_i} [\bar{u}^*(t)]^2 dt. \tag{10}$$

Note that OCP-2 is associated with the trajectory optimization only for the ith-segment while OCP-1 is associated with the optimization of the entire trajectory passing all the waypoints. OCP-2 is a typical guidance problem with terminal constraints of the impact angle and terminal lateral acceleration.

Now suppose that the trajectory solution to OCP-1 is known. The optimal waypoint passing angle and lateral acceleration at the ith-waypoint are denoted by $\theta_i^* = \theta(t_i^*)$ and $a_i^* = a(t_i^*)$, respectively, where t_i^* implies the optimal waypoint passing time. We then define the sets as follows

$$T^* \triangleq \{t_i^*,\ i = 0,1,\ldots,N\} \tag{11}$$

$$\Theta^* \triangleq \{\theta_i^*,\ i = 0,1,\ldots,N\} \tag{12}$$

$$A^* \triangleq \{a_i^*,\ i = 0,1,\ldots,N\}. \tag{13}$$

The following theorem provides the relationship between OCP-1 and OCP-2.

THEOREM 1 *If $\theta_i = \theta_i^*$, $a_i = a_i^*$, and $t_i = t_i^*$ for $i = 0,1,\ldots,N$, then $\bar{J}_i^* = J_i^*$ for $i = 1,\ldots,N$. Moreover, $\bar{u}^*(t) = u^*(t)$ for $t \in [t_{i-1}^*, t_i^*]$.*

Theorem 1 can be proved using the principle of optimality [13] in Appendix A. Theorem 1 implies that the optimal control history passing through all the waypoints can be obtained as a combination of the independent OCP-2's solutions for each segment if Θ^*, A^*, and T^* are given. We did not consider the case where some boundary conditions, which consist of waypoint passing angles and lateral accelerations, are prescribed. In this case, the prescribed boundary conditions can be treated as the optimal boundary conditions and it can easily be shown that Theorem 1 still holds.

Now suppose that $\bar{u}^*(t)$, the optimal control of OCP-2, is given by a state-feedback closed-form guidance law for a specified waypoint position (x_i, z_i);

$$\bar{u}_i^*(t) := \Gamma(t, x(t), z(t), \theta(t), a(t); \theta_i, a_i) \qquad \text{for} \quad t \in [t_{i-1}, t_i]. \tag{14}$$

Under the assumption that such a state-feedback law exists, we can consider the following parameter optimization problem.

POP-1: For the given t_i, find θ_i and a_i for $i = 0,1,\ldots,N$, which minimizes

$$\begin{aligned} \tilde{J} &= \sum_{i=1}^{N} \int_{t_{i-1}}^{t_i} [\bar{u}_i^*(t)]^2 dt \\ &= \sum_{i=1}^{N} \int_{t_{i-1}}^{t_i} [\Gamma(t, x(t), z(t), \theta(t), a(t); \theta_i, a_i)]^2 dt \end{aligned} \tag{15}$$

subject to (2).

POP-1 is that the problem of finding the optimal waypoint passing angles and lateral accelerations when the under the state-feedback optimal control law of OCP-2 is applied for each flight segment. The following theorem indicates the relationship between POP-1 and OCP-1.

THEOREM 2 *For the given T^*, let $\tilde{\Theta}^* \triangleq \{\tilde{\theta}_i^*,\ i = 0,1,\ldots,N\}$ and $\tilde{A}^* \triangleq \{\tilde{a}_i^*,\ i = 0,1,\ldots,N\}$ be the solution to POP-1, and the minimum cost $\tilde{J}^*$ given by*

$$\tilde{J}^* = \sum_{i=1}^{N} \int_{t_{i-1}^*}^{t_i^*} [\Gamma(t, x(t), z(t), \theta(t), a(t); \tilde{\theta}_i^*, \tilde{a}_i^*)]^2 dt. \tag{16}$$

Then, $\tilde{\Theta}^* = \Theta^*$, $\tilde{A}^* = A^*$ and $\tilde{J}^* = J^*$.

Proof of Theorem 2 is in Appendix A. Theorem 2 states that, for the given T^*, Θ^* and A^* can be obtained as the solution to POP-1 without solving OCP-1 if the closed-form state-feedback OGL for OCP-2 exists. Once Θ^* and A^* are specified, the energy optimal trajectory for OCP-1 can be produced by simply applying the state-feedback guidance law for OCP-2. While OCP-1 is a typical optimal control problem, POP-1 is a kind of parameter optimization problem. Since all boundary conditions are satisfied by the guidance law, POP-1 can be solved with significantly less numerical effort compared with OCP-1.

In this section, we suggest two different ways of producing the energy optimal trajectory passing through all the waypoints: one is obtained by the solution to OCP-1 via a numerical solver, another is by applying Γ, the state-feedback control law for OCP-2, to each flight segment with Θ^* and A^* which are given by the solution to POP-1. In order to guarantee the equivalence of both methods, a set of optimal waypoint passing times T^* should be specified before.

As mentioned before, if T^* is given as assumed in this section, the resultant optimal control obtained by both methods becomes globally energy-minimized control. One remaining issue that must be addressed to formalize POP-1 is how to determine T^*. Whenever an optimal guidance problem is formulated with the fixed terminal time, the obtained guidance law includes the terminal time typically considered in time-to-go. Γ also includes time-to-go in the control law. For the ith-segment, t_i^* becomes the terminal time for Γ. However, we need not necessarily prescribe t_i^* to apply Γ for every flight segment, because time-to-go in the OGLs can be calculated or approximated by a formulation in terms of state variables without direct consideration of the terminal time [10–12]. Widely used formula for time-to-go is the range over vehicle speed. In this way, with a great efficiency, the second method based on

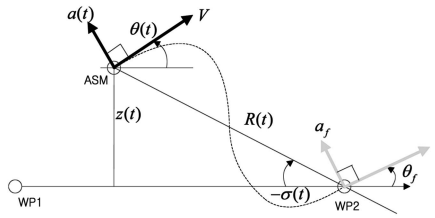

Fig. 3. Geometry of guidance to control of impact angle and terminal lateral acceleration.

POP-1 successfully produces a suboptimal trajectory passing though all the waypoints without involving T^*. Interestingly enough, however, numerical simulation results, which are dealt with in Section V, show that the second method produces globally energy-optimized control.

Instead of t_i^*, we can consider a user-specified t_i for OCP-1. Note that Theorems 1 and 2 are still true for the given t_i. In this case, the resultant trajectory passing through all the waypoints is not the globally energy-minimized trajectory but an energy optimal trajectory subjected to t_i. Although different energy optimal control history is obtained according to t_i, various kinds of meaningful missions such as simultaneous multi-vehicle formation and concurrent target attack are possible by properly choosing t_i.

III. OPTIMAL GUIDANCE LAWS

How to obtain a closed-form state-feedback guidance law as the solution to a linear quadratic (LQ) optimal control problem is addressed in this section. If the ASM is approximated by a 1st-order lag system, we need the OGL that can satisfy the terminal constraints on the impact angle and lateral acceleration. In this section, we introduce a new OGL for a 1st-order lag system. If a lag-free ASM is considered, the state variable of lateral acceleration disappears in (2), because $u = a$. In this case, the OGL with an impact angle constraint is required, as previously determined in [8], and can be derived from the law for a 1st-order lag system.

A. OGL with Terminal Constraints on Impact Angle and Lateral Acceleration

Fig. 3 shows a guidance geometry in which the ASM is guided to reach WP2 from WP1. All state variables are defined with respect to the reference line connecting WP1 and WP2. Assuming that θ is small, we linearize (2) as

$$\begin{aligned} \dot{x} &= V \\ \dot{z} &= V\theta \\ \dot{\theta} &= a/V \\ \dot{a} &= (\bar{u} - a)/\tau. \end{aligned} \tag{17}$$

Since the first equation in (17) does not affect the behavior of other state variables, it can be neglected in the analysis. By introducing a lateral velocity $v = V\theta$, state-space representation of (17) is given by

$$\dot{\xi} = A\xi + B\bar{u}, \qquad \xi(0) = \xi_0 \tag{18}$$

where

$$\xi = [z \quad v \quad a]^T, \qquad \xi_0 = [0 \quad v_0(= V\theta_0) \quad 0]^T \tag{19}$$

and

$$A = \begin{bmatrix} 0 & 1 & 0 \\ 0 & 0 & 1 \\ 0 & 0 & -1/\tau \end{bmatrix}, \qquad B = \begin{bmatrix} 0 \\ 0 \\ 1/\tau \end{bmatrix}. \tag{20}$$

OCP-2 then becomes the following LQ optimal control problem.

OCP-2(LQ): For a given t_f, find u that minimizes

$$\bar{J} = \frac{1}{2}\int_0^{t_f} \bar{u}^T(\tau)R\bar{u}(\tau)d\tau \tag{21}$$

where $R = 1$ and subject to the kinematics (18) with (20) and the terminal constraints

$$D\xi(t_f) = E \tag{22}$$

where

$$D = I_{3\times 3}, \qquad E = [0 \quad v_f(= V\theta_f) \quad a_f]^T. \tag{23}$$

A general state-feedback solution is given by the sweep method [14] as

$$\bar{u}^*(t) = R^{-1}B^TFG^{-1}(F^T\xi(t) - E) \tag{24}$$

where

$$\begin{aligned} \dot{F} &= -A^TF, \qquad F(t_f) = D^T \\ \dot{G} &= F^TBB^TF, \qquad G(t_f) = 0. \end{aligned} \tag{25}$$

Substituting (20) and (23) into (25) and integrating, we obtain

$$\begin{aligned} F &= \begin{bmatrix} f_{11} & f_{12} & f_{13} \\ f_{21} & f_{22} & f_{23} \\ f_{31} & f_{32} & f_{33} \end{bmatrix} \\ &\triangleq \begin{bmatrix} 1 & 0 & 0 \\ t_{\text{go}} & 1 & 0 \\ \tau t_{\text{go}} + \tau^2 e^{-t_{\text{go}}/\tau} - \tau^2 & \tau(1 - e^{-t_{\text{go}}/\tau}) & e^{-t_{\text{go}}/\tau} \end{bmatrix} \end{aligned} \tag{26}$$

and

$$G = \begin{bmatrix} g_{11} & g_{12} & g_{13} \\ g_{21} & g_{22} & g_{23} \\ g_{31} & g_{32} & g_{33} \end{bmatrix} \tag{27}$$

where

$$\begin{aligned} g_{11} &= -\tau^2 t_{\text{go}} + \tau t_{\text{go}}^2 - \tfrac{1}{3}t_{\text{go}}^3 + 2\tau^2 t_{\text{go}} e^{-t_{\text{go}}/\tau} \\ &\quad + \tfrac{1}{2}\tau^3(e^{-2t_{\text{go}}/\tau} - 1) \\ g_{12} &= g_{21} = \tau t_{\text{go}} - \tfrac{1}{2}t_{\text{go}}^2 + \tau(\tau - t_{\text{go}})e^{-t_{\text{go}}/\tau} \\ &\quad - \tfrac{1}{2}\tau^2(e^{-2t_{\text{go}}/\tau} + 1) \\ g_{13} &= g_{31} = t_{\text{go}}e^{-t_{\text{go}}/\tau} + \tfrac{1}{2}\tau(e^{-2t_{\text{go}}/\tau} - 1) \\ g_{22} &= -t_{\text{go}} + \tfrac{3}{2}\tau - \tau(2e^{-t_{\text{go}}/\tau} - \tfrac{1}{2}e^{-2t_{\text{go}}/\tau}) \\ g_{23} &= g_{32} = e^{-t_{\text{go}}/\tau} - \tfrac{1}{2}(e^{-2t_{\text{go}}/\tau} + 1) \\ g_{33} &= \tfrac{1}{2\tau}(e^{-2t_{\text{go}}/\tau} - 1). \end{aligned} \tag{28}$$

Here, t_{go} represents the time-to-go defined by $t_f - t$. Substituting (26) and (28) into (24) and using

$$\chi = \tanh\frac{t_{\text{go}}}{2\tau} \tag{29}$$

we finally obtain the optimal guidance law with terminal constraints on the impact angle and lateral acceleration (OGL-T&A) as

$$\begin{aligned} \bar{u}^* &= \Gamma(t, z(t), \theta(t), a(t); \theta_f, a_f) \\ &= \frac{1}{\Delta(t)}[C_1(t)z(t) + C_2(t)V\theta(t) + C_3(t)a(t) \\ &\qquad + C_4(t)V\theta_f + C_5(t)a_f] \end{aligned} \tag{30}$$

where

$$\begin{aligned} \Delta(t) &= 2(-t_{\text{go}} + 2\chi\tau)(\chi t_{\text{go}}^2 - 6\tau t_{\text{go}} + 12\tau^2\chi)t_{\text{go}} \\ C_1(t) &= 12(-t_{\text{go}} + 2\chi\tau)^2 \\ C_2(t) &= 2t_{\text{go}}[(\chi^2 + 3)t_{\text{go}}^2 - 18\chi\tau t_{\text{go}} + 24\tau^2\chi^2] \\ C_3(t) &= (\chi - 1)^2 t_{\text{go}}^4 + 4\tau(\chi^2 - 2\chi + 3)t_{\text{go}}^3 \\ &\quad + 12\tau^2(\chi^2 - 4\chi - 1)t_{\text{go}}^2 \\ &\quad + 48\chi\tau^3(\chi + 1)t_{\text{go}} - 48\chi^2\tau^4 \\ C_4(t) &= -2[(\chi^2 - 3)t_{\text{go}} + 6\chi\tau]t_{\text{go}}^2 \\ C_5(t) &= -[(1 - \chi^2)t_{\text{go}}^4 + 4\chi\tau t_{\text{go}}^3 - 12\tau^2(\chi^2 + 1)t_{\text{go}}^2 \\ &\quad + 48\chi\tau^3 t_{\text{go}} - 48\chi^2\tau^4]. \end{aligned} \tag{31}$$

The vehicle-to-target LOS angle $\sigma(t)$ can be approximated by

$$\sigma(t) \approx -z(t)/Vt_{\text{go}}. \tag{32}$$

Then, (30) can be rewritten

$$\begin{aligned} \bar{u}^* &= \frac{1}{\Delta(t)}[-VC_1(t)t_{\text{go}}\sigma(t) + C_2(t)V\theta(t) + C_3(t)a(t) \\ &\qquad + C_4(t)V\theta_f + C_5(t)a_f]. \end{aligned} \tag{33}$$

OGL-T&A can be independently applied for homing guidance of antitank or ASMs to attack the weak side of the target. Unlike previously studied impact-angle-control guidance laws [8, 15–18], OGL-T&A can control the terminal lateral acceleration without changing the terminal impact angle. By properly assigning a_f, OGL-T&A makes it possible to avoid saturation of lateral acceleration, which may occur in aerodynamically controlled missiles. By maximizing the lateral acceleration of an ASM in the terminal homing phase, without loss of impact-angle-control capability, aiming error of CIWS (close-in weapon system) against antiair threats can also be produced. Simulation results showing the basic properties of OGL-T&A are included in Appendix B. Another important application of OGL-T&A is in providing a closed-form state-feedback solution of OCP-2 to solve POP-1, as discussed in Section II.

B. OGL with Impact Angle Constraint for a Lag-Free System

If the vehicle's autopilot is fast enough or if the ratio of the time constant of the lag system to the flight time is small, the system lag can be ignored. If $\tau \to 0$, then $\chi \to 1$. OGL-T&A reduces to

$$\begin{aligned}\bar{u}^*(t) &= \Gamma(t, z(t), \theta(t); \theta_f) \\ &= C_R t_{\text{go}} + C_S \\ &= -\frac{V}{t_{\text{go}}^2}\left[\frac{6z(t)}{V} + 4t_{\text{go}}\theta(t) + 2t_{\text{go}}\theta_f\right] \end{aligned} \tag{34}$$

where C_R and C_S are constants [8] although they are expressed in terms of the state variables as

$$\begin{aligned} C_R &= -\frac{6V}{t_{\text{go}}^3}\left[\frac{2z(t)}{V} + t_{\text{go}}\theta(t) + t_{\text{go}}\theta_f\right] \\ C_S &= \frac{2V}{t_{\text{go}}^2}\left[\frac{3z(t)}{V} + t_{\text{go}}\theta(t) + 2t_{\text{go}}\theta_f\right]. \end{aligned} \tag{35}$$

Using (32), we can rewrite (34) as

$$\bar{u}^*(t) = \frac{V}{t_{\text{go}}}[6\sigma(t) - 4\theta(t) - 2\theta_f]. \tag{36}$$

We call the guidance law given by or OGL/0. Note that all the terms related to lateral acceleration in OGL-T&A disappear in OGL/0 because $\bar{u} = a$. In fact, OGL/0 is easily obtained by the sweep method. In this case, the optimal control problem is to find $\bar{u}^*$ minimizing the energy cost subject to

$$\dot{z} = V\theta, \qquad \dot{\theta} = \bar{u}/V \tag{37}$$

and

$$\theta(t_f) = \theta_f. \tag{38}$$

At $t = 0$, we have $z(0) = 0$, $\theta(0) = \theta_0$, and $t_{\text{go}} = t_f$. Hence, the constants C_R and C_S become

$$C_R = -\frac{6V}{t_f^2}(\theta_0 + \theta_f), \qquad C_S = \frac{2V}{t_f}(\theta_0 + 2\theta_f). \tag{39}$$

The optimal cost $\bar{J}^*$ defined in (21) is expressed as

$$\begin{aligned}\bar{J}^* &= \frac{1}{2}\int_0^{t_f}[\bar{u}^*(t)]^2 dt = \frac{1}{2}\int_0^{t_f}(C_R t_{\text{go}} + C_s)^2 dt \\ &= \frac{2V^2}{t_f}(\theta_0^2 + \theta_0\theta_f + \theta_f^2). \end{aligned} \tag{40}$$

It is noted that $\bar{J}^*$ is represented by a quadratic function of the initial launch angle and the terminal impact angle. By extending (40) to the multiple waypoints case, we can obtain an analytical expression of the cost function for POP-1.

IV. DETERMINATION OF THE OPTIMAL BOUNDARY CONDITIONS AT WAYPOINTS

A. POP-1 using OGL-T&A. 1st-Order Lag System Case

OGL-T&A given by (30) with (31) is a state-feedback guidance law with the time-varying coefficients represented in terms of time-to-go. As discussed in Section II, the time-to-go in the OGLs can be approximated by the range over the vehicle speed. In the ith-segment, let the time-to-go for OGL-T&A be given by

$$t_{\text{go}_i} = t_i^* - t \approx \frac{r_i}{V} \tag{41}$$

where r_i is the distance from the current ASM to the ith-waypoint.

In this way, $\tilde{J}$, the energy cost for POP-1, can be calculated from the guidance command histories without exact knowledge of t_i. Due to the complexity of OGL-T&A, numerical parameter optimization techniques are required to obtain Θ^* and A^*, the solution to POP-1. The conceptual procedure of finding the solution to POP-1 is as follows: Waypoint passing angles and lateral accelerations are arbitrarily assigned first. OGL-T&A is then applied to guide the ASM between waypoints. The cost $\tilde{J}$ can be calculated from the command histories of OGL-T&A. If $\tilde{J}$ is not the minimum, waypoint passing angles and lateral accelerations are updated. Repeat the procedure until $\tilde{J}$ is minimized.

B. POP-1 using OGL/0. Lag-Free System Case

In OCP-2(LQ), θ and σ are defined with respect to the reference line connecting WP1 to WP2, as

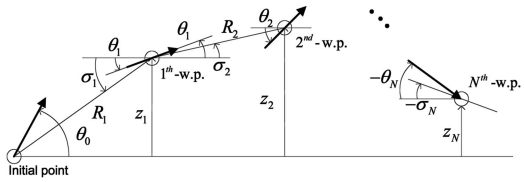

Fig. 4. Definitions of σ_i and R_i.

shown in Fig. 3. Let σ_i be the LOS angle of the line connecting the $(i-1)$th-waypoint and the ith waypoint as depicted in Fig. 4. Taking σ_i into account in (40), we obtain the analytic expression of the cost function for POP-1,

$$\begin{aligned}\tilde{J} = J &= \sum_{i=1}^{N}\int_{t_{i-1}}^{t_i}[\bar{u}^*(t)]^2dt \\ &= 4V^2\sum_{i=1}^{N}\frac{1}{\Delta t_i}[(\theta_{i-1}-\sigma_i)^2+(\theta_{i-1}-\sigma_i)(\theta_i-\sigma_i)+(\theta_i-\sigma_i)^2]\end{aligned} \tag{42}$$

where $\Delta t_i \triangleq t_i - t_{i-1}$.

For simplicity, we approximate Δt_i by the minimum flight time for each segment as

$$\Delta t_i \simeq R_i/V \tag{43}$$

where R_i is the distance between the $(i-1)$th- and the ith-waypoint. Then, is rewritten as

$$\begin{aligned}\tilde{J} \approx 4V^3\sum_{i=1}^{N}\frac{1}{R_i}[&(\theta_{i-1}-\sigma_i)^2+(\theta_{i-1}-\sigma_i)(\theta_i-\sigma_i) \\ &+(\theta_i-\sigma_i)^2].\end{aligned} \tag{44}$$

Here, σ_i and R_i are fixed and easily calculated from the waypoint positions. Note that the energy cost is approximated as a quadratic function of Θ, the waypoint passing angles. Thus, the necessary condition to minimize (44) yields a simple linear algebraic equation to calculate Θ^*. If some waypoint passing angles are prescribed, as illustrated in Fig. 5, the optimal trajectory can be independently obtained for each leg defined by a pair of waypoints. A cluster

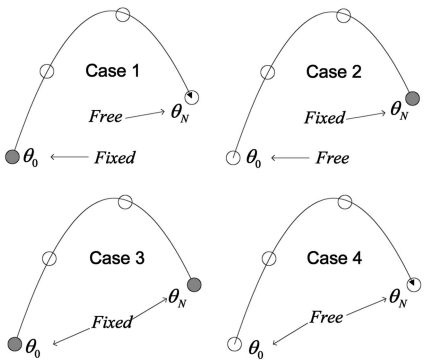

Fig. 5. Types of waypoint clusters.

of waypoints in each leg belongs to one of the following four cases:

Case 1 Fixed θ_0 and free θ_N

In this case, the unknown parameter vector is defined by

$$\Theta^* = [\theta_1^* \quad \theta_2^* \cdots \theta_{N-1}^* \quad \theta_N^*]^T \tag{45}$$

and Θ^* should satisfy the following necessary condition.

$$\left[\frac{\partial\tilde{J}}{\partial\theta_i}\right]_{\theta_i=\theta_i^*} = 0, \qquad i = 1,2,\ldots,N \tag{46}$$

or

$$0 = \begin{bmatrix} 2\theta_1^*\left(\frac{1}{R_1}+\frac{1}{R_2}\right)+\frac{\theta_2^*}{R_2}+\frac{\theta_0}{R_1}-\frac{3\sigma_1}{R_1}-\frac{3\sigma_2}{R_2} \\ \frac{\theta_1^*}{R_2}+2\left(\frac{1}{R_2}+\frac{1}{R_3}\right)\theta_2^*+\frac{\theta_3^*}{R_3}-\frac{3\sigma_2}{R_2}-\frac{3\sigma_3}{R_3} \\ \vdots \\ \frac{\theta_{N-1}^*}{R_{N-1}}+2\left(\frac{1}{R_{N-1}}+\frac{1}{R_N}\right)\theta_{N-1}^*+\frac{\theta_N^*}{R_N}-\frac{3\sigma_{N-1}}{R_{N-1}}-\frac{3\sigma_N}{R_N} \\ \frac{\theta_{N-1}^*}{R_N}+\frac{2\theta_N^*}{R_N}-\frac{3\sigma_N}{R_N} \end{bmatrix}. \tag{47}$$

From (47), we have

$$\Theta^* = R_A^{-1}\sigma_R \tag{48}$$

where

$$R_A \triangleq \begin{bmatrix} 2\left(\frac{1}{R_1}+\frac{1}{R_2}\right) & \frac{1}{R_2} & 0 & 0\ldots0 & 0 \\ \frac{1}{R_2} & 2\left(\frac{1}{R_2}+\frac{1}{R_3}\right) & \frac{1}{R_3} & 0\ldots0 & 0 \\ \vdots & \vdots & \vdots & \vdots & \vdots \\ 0 & 0 & \frac{1}{R_{N-1}} & 2\left(\frac{1}{R_{N-1}}+\frac{1}{R_N}\right) & \frac{1}{R_N} \\ 0 & 0 & 0 & \frac{1}{R_N} & \frac{2}{R_N} \end{bmatrix} \tag{49}$$

and

$$\sigma_R \triangleq 3\left[-\frac{\theta_0}{3R_1}+\frac{\sigma_1}{R_1}+\frac{\sigma_2}{R_2}\quad \frac{\sigma_2}{R_2}+\frac{\sigma_3}{R_3}\cdots\frac{\sigma_{N-1}}{R_{N-1}}+\frac{\sigma_N}{R_N}\quad \frac{\sigma_N}{R_N}\right]^T. \tag{50}$$

Case 2 Free θ_0 and fixed θ_N

Parameter vector

$$\Theta^* = [\theta_0^* \quad \theta_1^*\cdots\theta_{N-2}^* \quad \theta_{N-1}^*]^T. \tag{51}$$

Necessary condition

$$\left[\frac{\partial\tilde{J}}{\partial\theta_i}\right]_{\theta_i=\theta_i^*} = 0 \qquad \text{for} \quad i = 0,1,\ldots,N-1. \tag{52}$$

In a manner similar to Case 1, we have

$$R_A \triangleq \begin{bmatrix} \frac{2}{R_1} & \frac{1}{R_1} & 0 & 0\ldots0 & 0 \\ \frac{1}{R_1} & 2\left(\frac{1}{R_1}+\frac{1}{R_2}\right) & \frac{1}{R_2} & 0\ldots0 & 0 \\ \vdots & \vdots & \vdots & \vdots & \vdots \\ 0 & 0 & \frac{1}{R_{N-2}} & 2\left(\frac{1}{R_{N-2}}+\frac{1}{R_{N-1}}\right) & \frac{1}{R_{N-1}} \\ 0 & 0 & 0 & \frac{1}{R_{N-1}} & 2\left(\frac{1}{R_{N-1}}+\frac{1}{R_N}\right) \end{bmatrix} \tag{53}$$

and

$$\sigma_R \triangleq 3\left[\frac{\sigma_1}{R_1}\quad \frac{\sigma_1}{R_1}+\frac{\sigma_2}{R_2}\cdots\frac{\sigma_{N-2}}{R_{N-2}}+\frac{\sigma_{N-1}}{R_{N-1}}\quad \frac{\sigma_{N-1}}{R_{N-1}}+\frac{\sigma_N}{R_N}-\frac{\theta_N}{3R_N}\right]^T. \tag{54}$$

Case 3 Fixed θ_0 and fixed θ_N

Parameter vector

$$\Theta^* = [\theta_1^* \quad \theta_2^*\cdots\theta_{N-2}^* \quad \theta_{N-1}^*]^T. \tag{55}$$

Necessary condition

$$\left[\frac{\partial\tilde{J}}{\partial\theta_i}\right]_{\theta_i=\theta_i^*} = 0 \qquad \text{for} \quad i = 1,2,\ldots,N-1 \tag{56}$$

$$R_A \triangleq \begin{bmatrix} 2\left(\frac{1}{R_1}+\frac{1}{R_2}\right) & \frac{1}{R_2} & 0 & 0\ldots0 & 0 \\ \frac{1}{R_2} & 2\left(\frac{1}{R_2}+\frac{1}{R_3}\right) & \frac{1}{R_3} & 0\ldots0 & 0 \\ \vdots & \vdots & \vdots & \vdots & \vdots \\ 0 & 0 & \frac{1}{R_{N-2}} & 2\left(\frac{1}{R_{N-2}}+\frac{1}{R_{N-1}}\right) & \frac{1}{R_{N-1}} \\ 0 & 0 & 0 & \frac{1}{R_{N-1}} & 2\left(\frac{1}{R_{N-1}}+\frac{1}{R_N}\right) \end{bmatrix} \tag{57}$$

and

$$\sigma_R \triangleq 3\left[-\frac{\theta_0}{3R_1}+\frac{\sigma_1}{R_1}+\frac{\sigma_2}{R_2}\quad \frac{\sigma_2}{R_2}+\frac{\sigma_3}{R_3}\cdots\frac{\sigma_{N-2}}{R_{N-2}} + \frac{\sigma_{N-1}}{R_{N-1}}\quad \frac{\sigma_{N-1}}{R_{N-1}}+\frac{\sigma_N}{R_N}-\frac{\theta_N}{3R_N}\right]^T. \tag{58}$$

Case 4 Free θ_0 and free θ_N

Parameter vector

$$\Theta^* = [\theta_0^* \quad \theta_1^*\cdots\theta_{N-1}^* \quad \theta_N^*]^T. \tag{59}$$

Necessary condition

$$\left[\frac{\partial\tilde{J}}{\partial\theta_i}\right]_{\theta_i=\theta_i^*} = 0 \qquad \text{for} \quad i = 0,1,\ldots,N \tag{60}$$

$$R_A \triangleq \begin{bmatrix} \frac{2}{R_1} & \frac{1}{R_1} & 0 & 0\ldots0 & 0 \\ \frac{1}{R_1} & 2\left(\frac{1}{R_1}+\frac{1}{R_2}\right) & \frac{1}{R_2} & 0\ldots0 & 0 \\ \vdots & \vdots & \vdots & \vdots & \vdots \\ 0 & 0 & \frac{1}{R_{N-1}} & 2\left(\frac{1}{R_{N-1}}+\frac{1}{R_N}\right) & \frac{1}{R_N} \\ 0 & 0 & 0 & \frac{1}{R_N} & \frac{2}{R_N} \end{bmatrix} \tag{61}$$

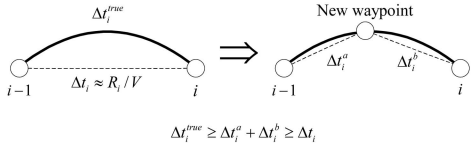

Fig. 6. Addition of new waypoint to improve accuracy of flight time calculation.

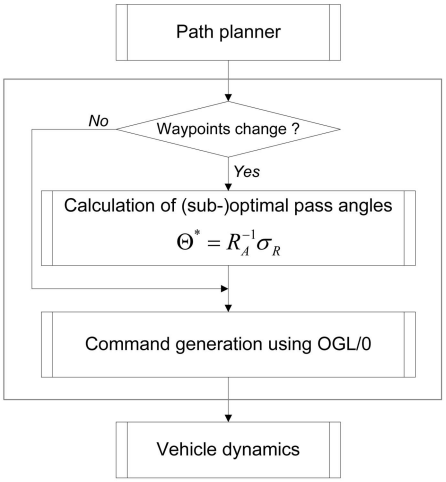

Fig. 7. Optimal waypoint guidance scheme.

and

$$\sigma_R \triangleq 3\left[\frac{\sigma_1}{R_1} \quad \frac{\sigma_1}{R_1}+\frac{\sigma_2}{R_2}\cdots\frac{\sigma_{N-1}}{R_{N-1}}+\frac{\sigma_N}{R_N} \quad \frac{\sigma_N}{R_N}\right]^T. \tag{62}$$

If the prescribed waypoints require a sharp corner, the approximation of the flight time given by (43) may not be appropriate and the error in the optimal solution calculated from the linear algebraic equations can be large. As illustrated in Fig. 6, adding new waypoints around the corner can alleviate this difficulty. Different from the path regulation methods, the trajectory produced by the proposed waypoint guidance synthesis may deviate from the desired path if wind is encountered. By assigning more waypoints along the trajectory, the wind effect can be overcome.

The optimal waypoint guidance scheme is shown in Fig. 7. First, the algorithm checks whether the waypoints in the remaining flight region have been changed. If there are some waypoint changes, the optimal waypoint passing angles are calculated again by using the linear algebraic equations. OGL/0 then produces the guidance command. The proposed guidance scheme produces the energy optimal trajectory in real time without any in-flight numerical optimization.

The proposed method does not require additional hardware beyond that required for guidance. Since the position of each waypoint is fixed and known before or in flight, a navigation system to measure the state of the ASM is sufficient to implement the proposed scheme.

V. NUMERICAL EXAMPLES

A. Definition of Mission Scenarios

We investigate the performance of the proposed methods via nonlinear simulations for two different mission scenarios. As shown in Figs. 8(a) and 9(a), nine waypoints on a plane are considered. The last waypoint (WP9) coincides with the initial point, and thus the entire flight path is divided into 9 flight segments. In scenario 1, there are no waypoints with prescribed boundary conditions, while in scenario 2 two waypoints have prescribed the passing angles and lateral accelerations: 45 deg and 0.0 m/s^2 on WP3, and -180 deg and 0.0 m/s^2 on WP7. The speed of the ASM is 100 m/s and remains constant during the flight. These mission scenarios seem unrealistic for an ASM, because the missile returns to the launch site again, but they reflect all possible cases of the prescribed boundary conditions. For an ASM approximated by a 1st-order lag system with $\tau = 1.0$ s, we first compare the trajectory solution to OCP-1 with the solution to POP-1 using OGL-T&A.

B. Comparison of OCP-1 and POP-1 using OGL-T&A. Trajectory Optimization

To solve OCP-1, we adopt the input parameter optimization technique [19]. In this technique, a dynamic optimal control problem can be converted to a static parameter optimization problem by parameterization of the control input. This technique has recently been widely used for trajectory optimization owing to its robustness of the initial guess of optimal control. After parameterization of the control input, typical parameter optimization methods such as sequential quadratic programming (SQP, [20]) and co-evolutionary augmented Lagrangian method (CEALM, [21]) can be directly employed to solve the problem.

In the optimization of OCP-1, for each segment, ten parameterized control inputs and the flight time are considered as the parameters to be optimized. That is, the parameter set is given by

$$X = \bigcup_{i=1}^{N} X_i \tag{63}$$

where $N = 9$ and

$$X_i \triangleq \{u_{i1}, u_{i2}, \ldots, u_{i10}, t_i\} \qquad \text{for the } i\text{th-segment.} \tag{64}$$

Therefore, the total number of parameters to be optimized is 99 for OCP-1.

For POP-1 using OGL-T&A, the parameter set contains 20 elements of the waypoint passing angles and lateral accelerations for scenario 1 and 16

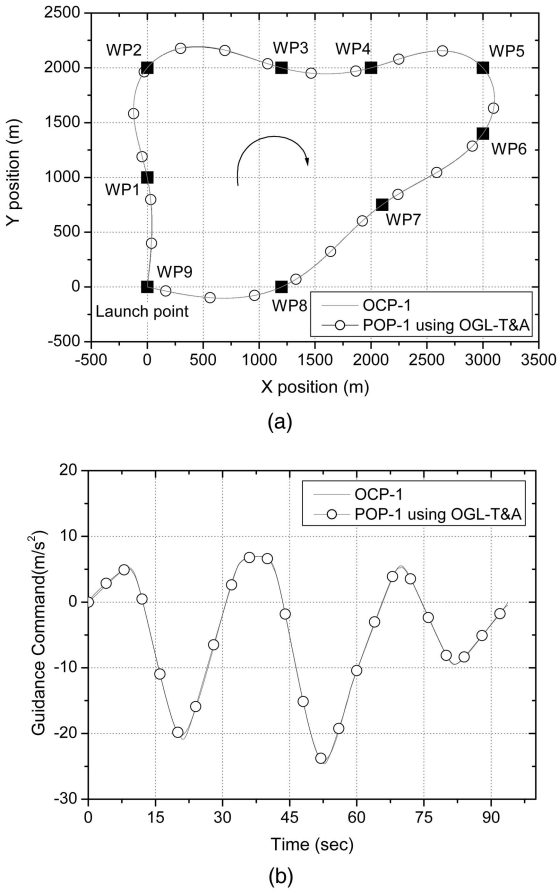

Fig. 8. Comparison of optimization results of scenario 1 for 1st-order ASM. (a) Energy optimal trajectories. (b) Profiles of guidance command magnitude.

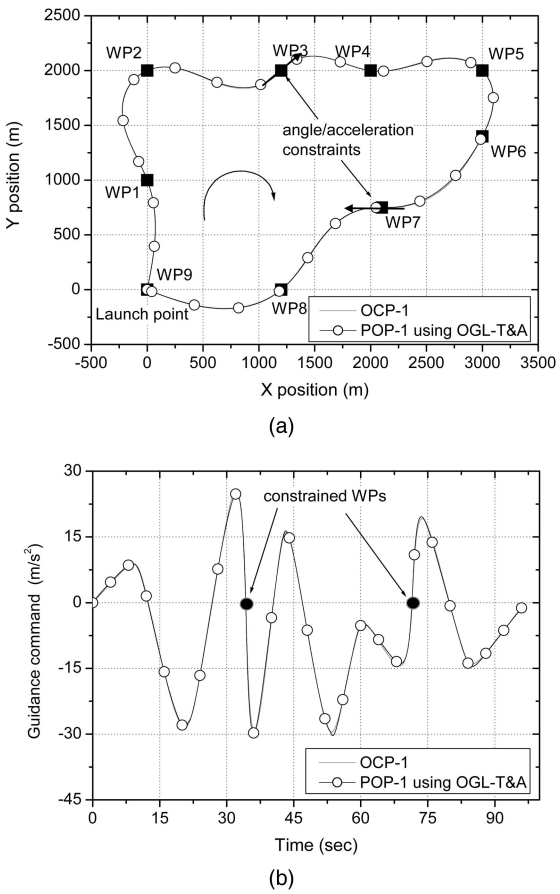

Fig. 9. Comparison of optimization results of scenario 2 for 1st-order lag ASM. (a) Energy optimal trajectories. (b) Profiles of guidance command magnitude.

elements for scenario 2:

$$X = \begin{cases} \{\theta_0, \theta_1, \ldots, \theta_9, a_0, a_1, \ldots, a_9\} & \text{for scenario 1} \\ \{\theta_0, \theta_1, \ldots, \theta_9, a_0, a_1, \ldots, a_9\} - \{\theta_3, \theta_7, a_3, a_7\} & \text{for scenario 2} \end{cases}. \tag{65}$$

The Runge-Kutta 4th-order method is used for the integration of (2) to calculate the cost and the violation of the terminal constraints for OCP-1. In POP-1, however, numerical integration is required only for the evaluation of the cost. The SQP method reported in [20] is adopted for both problems. The PC used for optimization has a 3.0 GHz Intel CPU with 512 MB RAM. All programs are coded by C++.

In the case of scenario 1, as shown in Table I, the optimal waypoint passing angles and lateral accelerations obtained from POP-1 are almost the same as those of OCP-1. The cost difference between the two methods is also negligible. However, it takes 485 s to solve OCP-1 while 166 s are required for POP-1. Comparison of the planar trajectory and guidance command profile for both methods is presented in Fig. 8. For scenario 2, it is also seen that the minimum cost and the optimal boundary conditions obtained from POP-1 are very similar to those of OCP-1, as shown in Table II. For both scenarios, the cost difference is less than 0.1%. However, it takes 698 s for OCP-1 while 191 s for POP-1. More calculation time is required for both methods due to the effect of the waypoints with prescribed boundary conditions. We observe from Fig. 9 that the magnitude of the maneuvering command is greater than that of scenario 1. The calculation times to solve OCP-1 are the minimal in our methodology presumably because the optimal control history is reused as the initial guess for both scenarios.

For OCP-1, the initial guess of $u(t)$ is very important to find the converged solution although the parameter optimization method proposed in [19] has been known to be robust to the initial guess. Several trials of the initial guess of the input control are always carried out to obtain the solution of OCP-1. On the contrary, the initial guess of the boundary conditions for POP-1 is very easy, because the geometrical distribution of waypoints provides insight into the proper choice of the initial waypoint passing angles and lateral accelerations. In most cases, the optimal solution can be obtained at the first

TABLE I
J^*, Θ^*, A^* of Scenario 1 for 1st-Order Lag ASM

	OCP-1	POP-1(OGL-T&A)
J^*	5058.60	5062.86
θ_0^* (deg)/a_0^* (m/s^2)	83.88/0.00	83.26/0.00
θ_1^*/a_1^*	101.47/4.69	101.66/4.35
θ_2^*/a_2^*	51.32/ − 20.24	50.96/ − 20.05
θ_3^*/a_3^*	−15.23/5.31	−15.11/5.30
θ_4^*/a_4^*	15.27/5.42	15.18/5.10
θ_5^*/a_5^*	−48.44/ − 24.01	−48.63/ − 23.76
θ_6^*/a_6^*	−123.68/ − 13.32	−123.83/ − 13.40
θ_7^*/a_7^*	−143.69/5.50	−143.46/5.16
θ_8^*/a_8^*	−155.25/ − 9.37	−155.46/9.47
θ_9^*/a_9^*	167.14/ − 0.47	167.04/ − 0.07

TABLE II
J^*, Θ^*, A^* of Scenario 2 for 1st-Order Lag ASM

	OCP-1	POP-1 (OGL-T&A)
J^*	11727.67	11780.23
θ_0^* (deg)/a_0^* (m/s^2)	79.40/0.00	78.76/0.00
θ_1^*/a_1^*	109.81/8.10	110.34/7.72
θ_2^*/a_2^*	23.48/ − 27.60	23.73/ − 27.02
θ_3^*/a_3^*	45/0.0: Given	
θ_4^*/a_4^*	−7.20/16.11	−7.77/15.71
θ_5^*/a_5^*	−46.48/ − 29.51	−45.43/ − 29.50
θ_6^*/a_6^*	−115.84/ − 5.37	−116.91/ − 5.76
θ_7^*/a_7^*	−180/0.0: Given	
θ_8^*/a_8^*	−140.48/ − 13.34	−139.57/ − 13.21
θ_9^*/a_9^*	159.07/ − 0.72	158.36/ − 0.62

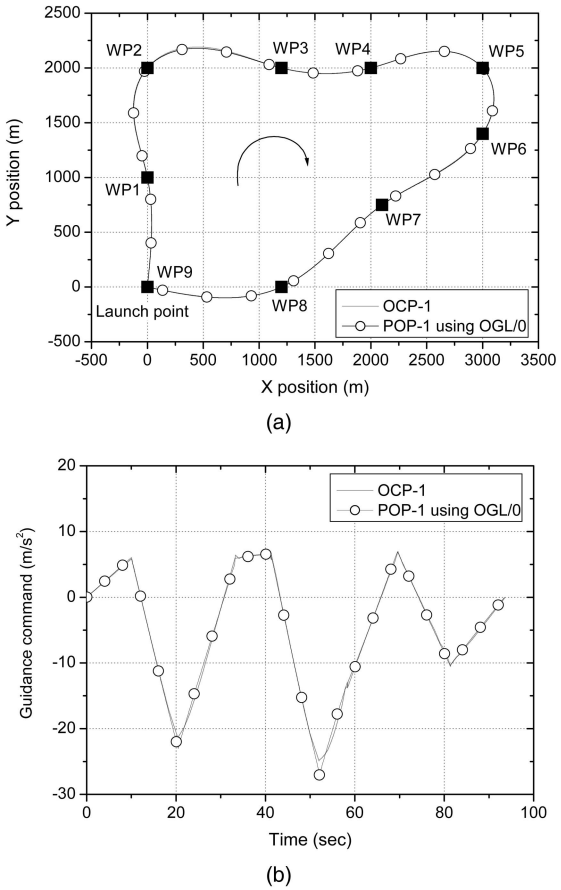

Fig. 10. Comparison of optimization results of scenario 1 for lag-free ASM. (a) Energy optimal trajectories. (b) Profiles of guidance command magnitude.

trial in POP-1. Hence, the proposed method reduces the numerical effort to find the optimal trajectory even more than as revealed by comparisons of the calculation time.

C. Real-Time Trajectory Generation: POP-1 using OGL/0

For the same scenarios, we compare trajectory solutions for a lag-free ASM: the solution of OCP-1 and the solution of POP-1 using OGL/0. Here, the linear algebraic equations to obtain Θ^* are used for the latter case. Since scenario 1 does not have any prescribed waypoint passing angles, it corresponds to Case 4 defined in Section IVB. In scenario 2, the entire flight path is divided into three distinct legs: Case 2 from WP1 to WP3, Case 3 from WP3 to WP7, and Case 1 from WP7 to WP9. Solving OCP-1 is very similar to that of the 1st-order lag case except the system lag is neglected in the dynamic constraint given by (2).

For scenario 1, both methods also produce almost the same optimal waypoint passing angles as shown in Table III. The minimum cost is obtained by OCP-1. The cost difference between OCP-1 and POP-1 using OGL/0 is less than 0.6%. If PNG with $N = 3$ is applied to this scenario, the required cost is 7043.0, which is 43.5% more than OCP-1. From Fig. 10, we observe that command profiles and trajectories obtained from both optimization methods are similar. Calculation for OCP-1 takes 278 s but the proposed method requires only several milliseconds.

For scenario 2, it takes 615 s to obtain the optimal solution to OCP-1. Again, the proposed method requires only a few milliseconds to obtain near optimal results, as shown in Table IV. In this example, the cost difference between the proposed method and OCP-1 is only 0.3%. PNG cannot be applied to this scenario since it cannot achieve the prescribed waypoint passing angles. Fig. 11 shows that command profiles and trajectories obtained from both optimization methods are almost the same. Different from the case of a 1st-order lag vehicle, as shown in Fig. 9(b), guidance command discontinuities at the prescribed waypoints are observed from Fig. 11(b). It is clear that real-time calculation of the energy optimal trajectory is possible if the lag of the vehicle is neglected.

TABLE III
J^*, Θ^* of Scenario 1 for Lag-Free ASM

	OCP-1	POP-1(OGL/0)[86]
J^*	4907.62	4937.00
θ_0^* (deg)	84.35	84.17
θ_1^*	101.17	101.67
θ_2^*	50.96	49.15
θ_3^*	−14.65	−14.28
θ_4^*	14.85	14.84
θ_5^*	−48.31	−48.92
θ_6^*	−123.21	−122.36
θ_7^*	−143.92	−144.00
θ_8^*	−155.42	−155.92
θ_9^*	167.70	167.96

TABLE IV
J^*, Θ^* of Scenario 2 for Lag-Free ASM

	OCP-1	POP-1 (OGL/0)
J^*	9635.03	9664.06
θ_0^* (deg)	81.46	82.08
θ_1^*	106.91	105.85
θ_2^*	30.78	34.54
θ_3^*	45: Given	
θ_4^*	−2.20	−1.92
θ_5^*	−46.90	−47.62
θ_6^*	−116.79	−116.47
θ_7^*	−180: Given	
θ_8^*	−144.32	−145.53
θ_9^*	162.04	162.77

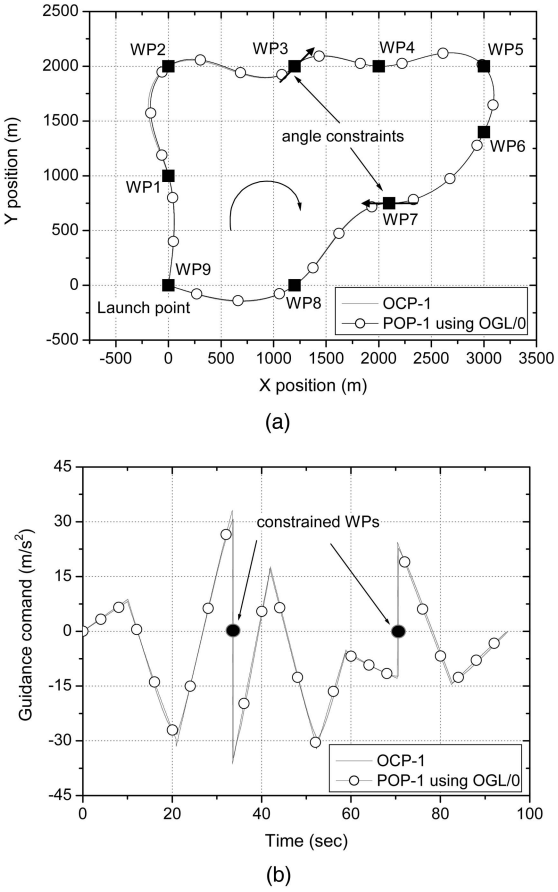

Fig. 11. Comparison of optimization results of scenario 2 for lag-free ASM. (a) Energy optimal trajectories. (b) Profiles of guidance command magnitude.

Note that the numerical solutions for OCP-1 in Section VB have been obtained without consideration of any specified waypoint passing time t_i. Hence, OCP-1's trajectories for scenario 1 and scenario 2 are globally energy minimized, respectively. On the other hand, as discussed in Section II, the energy optimal control produced by the proposed method may vary according to how to assign a passing time to each waypoint. Interestingly enough, the numerical simulation results show that the OGLs using Θ^* and A^* obtained by solving POP-1 produces the globally energy-optimized trajectory. It seems that if the time-to-go in OGL-T&A and OGL/0 is approximated by the range over vehicle speed, the proposed method produces the globally energy-optimized control as t_i in POP-1 disappears.

VI. CONCLUDING REMARKS

In this paper, we suggest new waypoint guidance synthesis methods involving efficient trajectory optimization. The basic concept underlying the proposed method is that the energy optimal trajectory passing through all the waypoints can be obtained by applying OGLs if the boundary conditions at the waypoints are properly assigned.

For a 1st-order lag vehicle, OGL-T&A, that is, the energy OGL with terminal constraints on the impact angle and lateral acceleration, can be used for the trajectory optimization. The proposed method is not only robust to the initial guess, but also efficient in terms of calculation time. The proposed method, however, always produces a suboptimal trajectory due to the assumptions of a 1st-order lag vehicle and linearized dynamics. Hence, the proposed method may be exploited for providing a preliminary analysis of mission trajectory before the detailed trajectory optimization considering the real vehicle dynamics and environment is sought.

In the case where the vehicle can be approximated by a lag-free system, OGL/0, the OGL with an impact angle constraint, can be applied for waypoint guidance. Unlike the 1st-order lag system, the waypoint passing angles to make the resultant trajectory energy optimal can be solved by using the linear algebraic equations. The proposed method produces the energy optimal trajectory passing all the waypoints in real time. As most missiles adopt guidance laws obtained without considering the lag of

the system, the proposed waypoint guidance synthesis method for sea skimming ASMs takes advantage of both robustness to in-flight change of waypoints and energy optimality of the resultant trajectory.

APPENDIX A. PROOF OF THE THEOREMS

THEOREM 1 *If $\theta_i = \theta_i^*$, $a_i = a_i^*$, and $t_i = t_i^*$ for $i = 0,1,\ldots,N$, then $\bar{J}_i^* = J_i^*$ for $i = 1,\ldots,N$. Moreover, $\bar{u}^*(t) = u^*(t)$ for $t \in [t_{i-1}^*, t_i^*]$.*

PROOF For the Nth-segment, from the principle of optimality [9], J_N^* with $u^*(t)$ is the minimum cost for OCP-1. From the assumption, the initial conditions and terminal constraints of OCP-2 are identical to the boundary conditions of OCP-1 for the Nth-segment. If $\bar{u}^*(t) \neq u^*(t)$, there exists another optimal control for OCP-2. This contradicts that $\bar{u}^*(t)$ is the optimal control for OCP-2. Hence, $\bar{u}^*(t) = u^*(t)$ for $t \in [t_{N-1}^*, t_N^*]$ and $\bar{J}_N^* = J_N^*$. For $[t_{N-2}^*, t_N^*]$, also from the principle of optimality, we see that $J_{N-1}^* + J_N^*$ is the minimum cost. Therefore, $J_{N-1}^* + J_N^* \leq \bar{J}_{N-1}^* + \bar{J}_N^*$. Since $\bar{J}_N^* = J_N^*$, we have $J_{N-1}^* \leq \bar{J}_{N-1}^*$. This contradicts $\bar{J}_{N-1}^*$ being the minimum cost of OCP-2 if $\theta_i = \theta_i^*$, $a_i = a_i^*$, and $t_i = t_i^*$ for $i = N-2, N-1$. Hence, $J_{N-1}^* = \bar{J}_{N-1}^*$ and $\bar{u}^*(t) = u^*(t)$ for $t \in [t_{N-2}^*, t_{N-1}^*]$. By repeating the procedure up to the first segment, we can prove the theorem.

THEOREM 2 *For the given T^*, let $\tilde{\Theta}^* \triangleq \{\tilde{\theta}_i^*, i = 0,1,\ldots,N\}$ and $\tilde{A}^* \triangleq \{\tilde{a}_i^*, i = 0,1,\ldots,N\}$ be the solution to POP-1, and the minimum cost $\tilde{J}^*$ given by*

$$\tilde{J}^* = \sum_{i=1}^{N} \int_{t_{i-1}^*}^{t_i^*} [\Gamma(t, x(t), z(t), \theta(t), a(t); \tilde{\theta}_i^*, \tilde{a}_i^*)]^2 dt. \tag{66}$$

Then, $\tilde{\Theta}^* = \Theta^*$, $\tilde{A}^* = A^*$. Thus, $\tilde{J}^* = J^*$.

PROOF Suppose that $\tilde{\Theta}^* \cup \tilde{A}^* \neq \Theta^* \cup A^*$; then

$$\tilde{J}^* < \sum_{i=1}^{N} \int_{t_{i-1}^*}^{t_i^*} [\Gamma(t, x(t), z(t), \theta(t), a(t); \theta_i^*, a_i^*)]^2 dt. \tag{67}$$

Recall that Γ is the state-feedback optimal control law obtained from OCP-2. By Theorem 1, if Θ^* and A^* are used for OCP-2, we have

$$\sum_{i=1}^{N} \int_{t_{i-1}^*}^{t_i^*} [\Gamma(t, x(t), z(t), \theta(t), a(t); \theta_i^*, a_i^*)]^2 dt = \sum_{i=1}^{N} \bar{J}_i^* = J^*. \tag{68}$$

The inequality given by can be satisfied only by violating the fact that J^* is the minimum cost for OCP-1. Hence, by contradiction, the theorem is true.

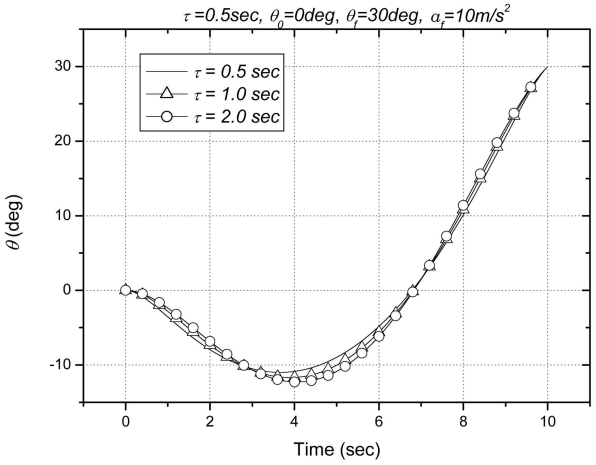

Fig. 12. Linear simulation: comparison of flight path angle history for various τ.

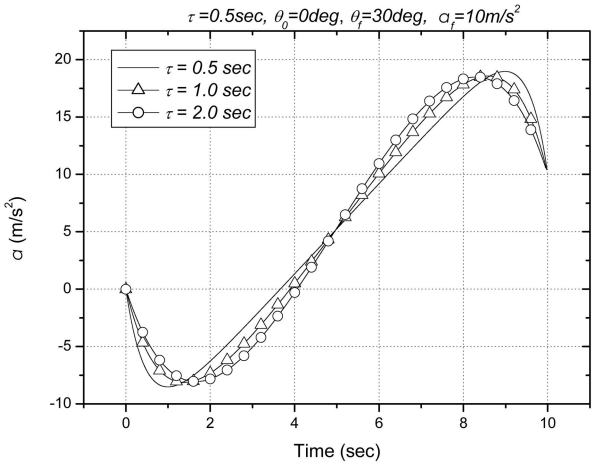

Fig. 13. Linear simulation: comparison of lateral acceleration history for various τ.

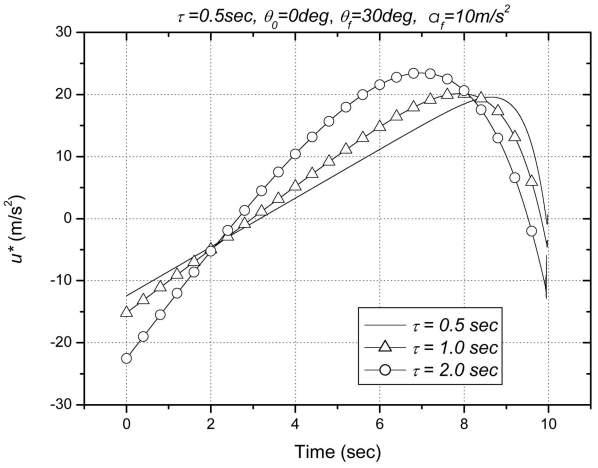

Fig. 14. Linear simulation: comparison of guidance command history for various τ.

APPENDIX B. NUMERICAL EXAMPLES OF OGL-T&A

To investigate the effect of τ on the guidance system, linear simulations using OGL-T&A given by (30) are performed. Simulation conditions are

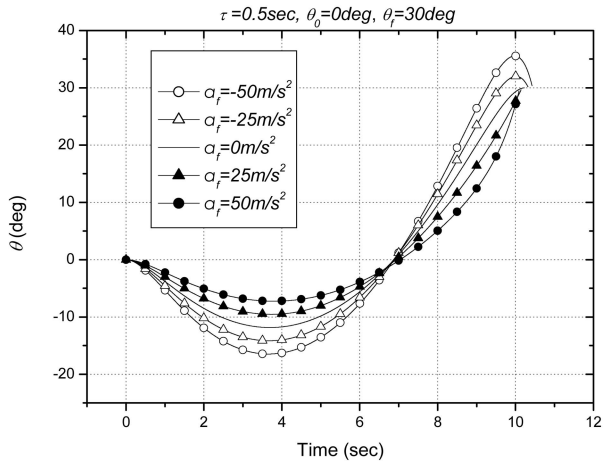

Fig. 15. Nonlinear simulation: comparison of flight path angle history for various a_f.

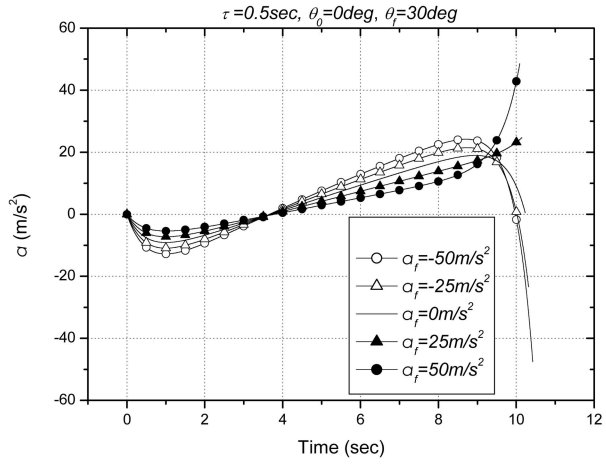

Fig. 16. Nonlinear simulation: comparison of lateral acceleration history for various a_f.

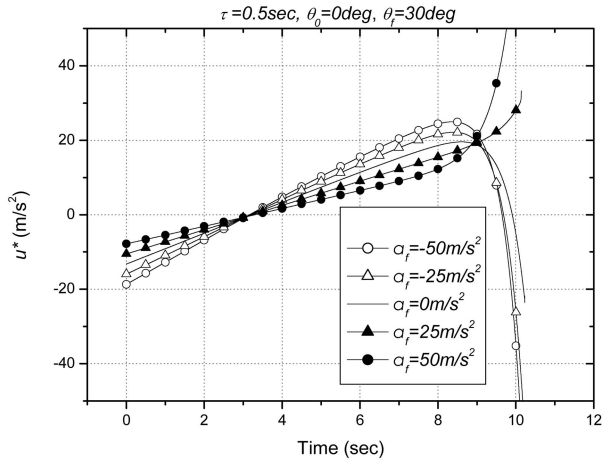

Fig. 17. Nonlinear simulation: comparison of guidance command history for various a_f.

set as $V = 100$ m/s^2, $t_f = 10$ s, $\theta_0 = 0$ deg, $\theta_f = 30$ deg, and $a_f = 10$ m/s^2. We observe from Fig. 12 that the flight path angle histories are not changed substantially according to τ. As shown in Figs. 13 and 14, however, guidance command and acceleration

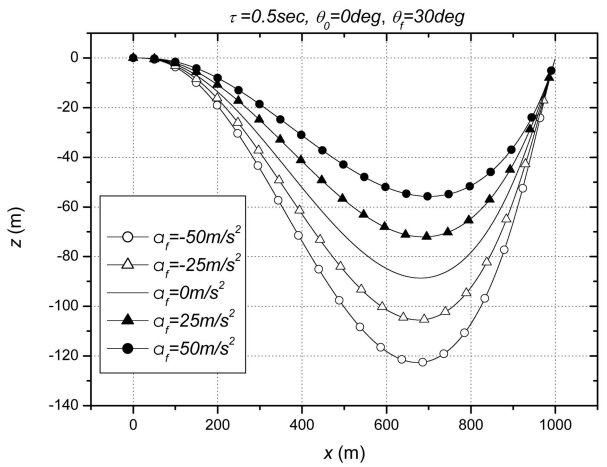

Fig. 18. Nonlinear simulation: comparison of planar trajectory history for various a_f.

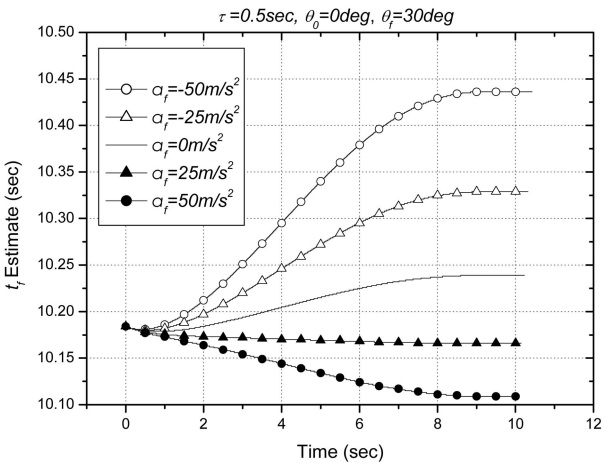

Fig. 19. Nonlinear simulation: comparison of history of estimated t_f $(= t + t_{\text{go}})$ for various a_f.

are largely affected by τ, i.e., much acceleration is needed in order to follow the guidance command. As τ becomes smaller, the linear region of the guidance command is enlarged (see Fig. 14). It is expected that the command produced by OGL-T&A will approach that of OGL/0 [4].

Figs. 15–19 show nonlinear simulation results for various a_f, where the time-to-go calculation method 2 suggested in [4] is used to calculate t_{go} in OGL-T&A given by (33). Here, $V = 100$ m/s^2, $\theta_0 = 0$ deg, and $\theta_f = 30$ deg are used for the simulations. The initial distance between the missile and the target is 1000 m. As shown in Fig. 15, the desired impact angle ($\theta_f = 30$ deg) is successfully achieved regardless of the assigned a_f. Fig. 16 shows that the terminal lateral acceleration history is severely changed according to a_f although all assigned a_f are satisfied. Acceleration saturation can be avoided by properly choosing a_f without changing the impact angle. OGL-T&A enhances the survivability of the ASM by maneuvering in the terminal homing phase against ship-borne antiair threats such as CIWS.

However, a large guidance command may cause system instability as shown in Fig. 17. We observe from Fig. 18 that the trajectory deviates less from the initial LOS as a_f increases. This is largely due to the fact that the turn curvature should be small to achieve large lateral acceleration. Note that method 2 provides very accurate time-to-go estimates, within 3% error, although it is designed for OGL/0 for a lag-free vehicle, as shown in Fig. 19.

REFERENCES

[1] Spangelo, I., and Egeland, O.
Generation of energy-optimal trajectories for an autonomous underwater vehicle.
In *Proceedings of the l992 IEEE International Conference on Robotics and Automation*, May 1992, 2107–2112.

[2] Moon, G., and Kim, Y.
Optimum flight path design passing through waypoints for autonomous flight control system.
In *Proceedings of the 2003 AIAA Guidance, Navigation, and Control Conference and Exhibit*, Aug. 2003.

[3] Ben-Asher, J. Z.
Optimal trajectories for an unmanned air-vehicle in the horizontal plane.
Journal of Aircraft, **32**, 3 (1995), 677–680.

[4] Shapira, I., and Ben-Asher, J. Z.
Near-optimal horizontal trajectories for autonomous air vehicles.
Journal of Guidance, Control, and Dynamics, **20**, 4 (1997), 745–741.

[5] Zarchan, P.
Tactical and Strategic Missile Guidance (4th ed.).
New York: AIAA, 2003, 11–15.

[6] Bakaric, V., Vukic, Z., and Antonic, R.
Improved basic planar algorithm of vehicle guidance through waypoints by the line of sight.
In *Proceedings of the IEEE International Symposium on Communications and Signal Processing*, 2004, 541–544.

[7] Whang, I. H., and Whang, T. W.
Horizontal waypoint guidance design using optimal control.
IEEE Transactions on Aerospace and Electronic Systems, **38**, 3 (July 2002), 1116–1120.

[8] Ryoo, C. K., Cho, H., and Tahk, M. J.
Optimal guidance laws with terminal impact angle constraint.
Journal of Guidance, Control, and Dynamics, **28**, 4 (2005), 724–732.

[9] Rew, D. Y., Tahk, M. J., and Cho, H. J.
Short-time stability of proportional navigation guidance loop.
IEEE Transactions on Aerospace and Electronic Systems, **32**, 3 (1996), 1107–1115.

[10] Lee, G. K. F.
Estimation of the time-to-go parameter for air-to-air missiles.
Journal of Guidance, Control, and Dynamics, **8**, 2 (1985), 262–266.

[11] Hull, D. G., Radke, J. J., and Mack, R. E.
Time-to-go prediction for homing missiles based on minimum-time intercepts.
Journal of Guidance, Control, and Dynamics, **14**, 5 (1991), 865–871.

[12] Tahk, M. J., and Ryoo, C. K., and Cho, H.
Recursive time-to-go estimation for homing guidance missiles.
IEEE Transactions on Aerospace and Electronic Systems, **38**, 1 (2002), 13–24.

[13] Kirk, D. E.
Optimal Control Theory-An Introduction.
Englewood Cliffs, NJ: Prentice-Hall, 1970, 54–55.

[14] Bryson, A. E., Jr., and Ho, Y-C.
Applied Optimal Control.
New York: Wiley, 1975, 158–167.

[15] Kim, M., and Grider, K. V.
Terminal guidance for impact attitude angle constrained flight trajectories.
IEEE Transactions on Aerospace and Electronic Systems, **AES-9**, 6 (1973), 852–859.

[16] Kim, B. S., Lee, J. G., and Han, H. S.
Biased PNG law for impact with angular constraint.
IEEE Transactions on Aerospace and Electronic Systems, **34**, 1 (1998), 277–288.

[17] Ohlmeyer, E. J., an Phillips, C. A.
Generalized vector explicit guidance.
Journal of Guidance, Control, and Dynamics, **29**, 2 (2006), 261–268.

[18] Ryoo, C. K., Cho, H., and Tahk, M. J.
Time-to-go weighted optimal guidance law with impact angle constraints.
IEEE Transactions on Control Systems Technology, **14**, 3 (2006), 483–492.

[19] Hull, D. G.
Conversion of optimal control problems into parameter optimization problems.
Journal of Guidance, Control, and Dynamics, **20**, 1 (1997), 57–60.

[20] Lawrence, C., Zhou, K. L., and Tits, A. L.
User's Guide for CFSQP Version 2.5: A C Code for Solving (Large Scale) Constrained Nonlinear (Minmax) Optimization Problems, Generating Iterates Satisfying All Inequality Constraints.
Institute for Systems Research, University of Maryland, 1997.

[21] Tahk, M. J., and Sun, B. C.
Co-evolutionary augmented Lagrangian methods for constrained optimization.
IEEE Transactions on Evolutionary Computation, **4**, 2 (2000), 114–124.

Chang-Kyung Ryoo received the B.S. degree in aerospace engineering from Inha University, Korea, in 1989. He received the M.S. and Ph.D. degrees in aerospace engineering from the Korea Advanced Institute of Science and Technology, in 1991 and 2006, respectively.

From 1991 to 2006 he was a research engineer with the Agency for Defense Development, Korea. Since 2006, he has been an assistant professor in the Department of Aerospace Engineering at Inha University. His recent research areas are advanced missile and UAV guidance, nonlinear systems control, and trajectory optimization.

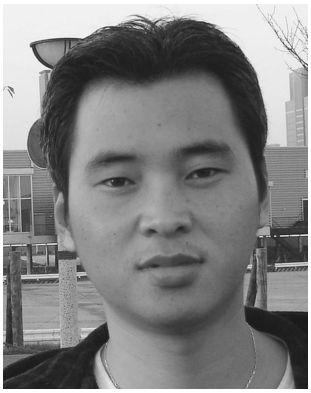

Hyo-Sang Shin received his B.Sc. in aerospace engineering from the Pusan National University in 2004, and his M.Sc. in guidance and control engineering from the Korea Advanced Institute of Science and Technology (KAIST) in 2006.

He is a Ph.D. student in the Department of Aerospace Engineering at KAIST and has been a visiting researcher student in the Department of Informatics and Sensors at Cranfield University's Shrivenham Campus since 2007. His primary research interests include robust and nonlinear control theories, sensor based navigation, guidance design for missiles, estimation methods, cooperative control for UAVs, and conflict detection and resolution algorithm.

Min-Jea Tahk was born in Daegu, Korea in 1954. He received the B.S. degree in aeronautics from Seoul National University in 1976, and the M.S. and Ph.D. degrees in aerospace engineering from the University of Texas at Austin, in 1983 and 1986, respectively.

He was a research engineer at the Agency for Defense Development, Daejeon, Korea, from 1976 to 1981, and Research Scientist at Integrated Systems, Inc., Santa Clara, CA, from 1987 to 1989. Currently, he is professor in the Department of Aerospace Engineering of Korea Advanced Institute of Science and Technology, Daejeon, Korea. His research interests include guidance and control of aerospace vehicles, fuzzy control, neural network adaptive control, and evolutionary computation for optimization.